Pure kinetic inductance coupling for cQED with flux qubits

Simon Geisert,[1] Soeren Ihssen,[1] Patrick Winkel,[1,2,3] Martin Spiecker,[1] Mathieu Fechant,[1] Patrick Paluch,[1,4] Nicolas Gosling,[1] Nicolas Zapata,[1] Simon Günzler,[1] Dennis Rieger,[1,4] Denis Bénâtre,[1] Thomas Reisinger,[1] Wolfgang Wernsdorfer,[1,4] and Ioan M. Pop[1,4,5,a)]

AFFILIATIONS

[1]IQMT, Karlsruhe Institute of Technology, 76131 Karlsruhe, Germany
[2]Departments of Applied Physics and Physics, Yale University, New Haven, Connecticut 06511, USA
[3]Yale Quantum Institute, Yale University, New Haven, Connecticut 06511, USA
[4]PHI, Karlsruhe Institute of Technology, 76131 Karlsruhe, Germany
[5]Physics Institute 1, Stuttgart University, 70569 Stuttgart, Germany

[a)]Author to whom correspondence should be addressed: ioan.pop@kit.edu

ABSTRACT

We demonstrate a qubit-readout architecture where the dispersive coupling is entirely mediated by a kinetic inductance. This allows us to engineer the dispersive shift of the readout resonator independent of the qubit and resonator capacitances. We validate the pure kinetic coupling concept and demonstrate various generalized flux qubit regimes from plasmon to fluxon, with dispersive shifts ranging from 60 kHz to 2 MHz at the half-flux quantum sweet spot. We achieve readout performances comparable to conventional architectures with quantum state preparation fidelities of 99.7% and 92.7% for the ground and excited states, respectively, and below 0.1% leakage to non-computational states.

The ability to convert model Hamiltonians into programmable physical systems is a stepping stone for quantum information processing. Circuit quantum electrodynamics (cQED) has been at the forefront of quantum hardware development over the past two decades,[1,2] benefitting from the freedom to design various microelectronic circuit elements such as qubits, control, readout, and coupler structures from the same basic building blocks. This has led to the development of increasingly complex quantum processors[3–7] and facilitated the exploration of fundamental quantum effects.[8–14]

Dispersive coupling between qubits and harmonic oscillators is a pivotal resource for cQED, enabling single shot readout,[15–18] the creation of non-classical photonic states,[19,20] reservoir engineering for qubit state preparation,[21,22] and even the autonomous stabilization of entangled states.[23] Conventionally, dispersive coupling is mediated via electromagnetic interaction, most commonly using the electric field and a coupling capacitor. However, in complex devices, stray capacitors inevitably introduce unwanted crosstalk, renormalize the dispersive shift and even induce undesired electromotive forces across nonlinear elements in the presence of alternating magnetic fields or field gradients.[24] In order to reduce the number of spurious electromagnetic modes and parasitic capacitances, several mitigation strategies are currently being developed in the community, including deep silicon vias,[25–27] flip-chip architectures,[4,5,26,28] and chiplets.[29,30]

Here, we present an alternative coupling approach that implements dispersive readout via pure kinetic inductance coupling between a generalized flux qubit and a harmonic oscillator and enables the complete suppression of capacitive coupling. We achieve this by designing a three-island circuit with two normal modes, i.e., qubit and resonator, coupled solely by a kinetic inductance. While the kinetic inductance can be realized with Josephson junction (JJ) arrays, we demonstrate the concept with a high kinetic inductance material, namely granular aluminum (grAl).[31,32] The circuit's symmetry effectively eliminates capacitive contributions to the qubit-readout interaction, rendering the coupling local.

To design the qubit-readout coupling, we follow three design rules that will be expanded in the following paragraphs. First, we use the minimally required complexity for two electromagnetic modes, i.e., three circuit nodes. Second, we allocate different roles to the common

and differential modes to implement the resonator and qubit. The qubit mode is obtained by connecting two nodes with a JJ. The electromagnetic mode that charges these nodes out of phase inherits a large anharmonicity from the JJ, while the orthogonal in-phase mode remains harmonic. Third, electric field coupling between the resonator and the qubit is eliminated by enforcing symmetric capacitors for the circuit nodes connecting the JJ, resulting in a permutation invariance of the capacitance matrix for these nodes.

In Fig. 1(a), we present our lumped-element circuit design consisting of three superconducting islands, i.e., circuit nodes 1, 2, and 3, connected via kinetic inductors made of grAl. The resulting superconducting loop, interrupted by the JJ and threaded by external flux Φ_{ext},

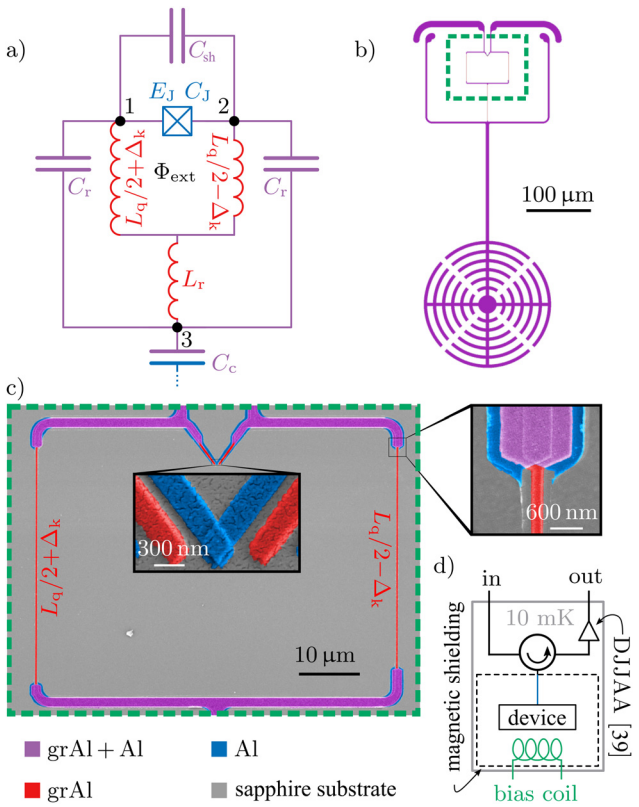

FIG. 1. Qubit-readout circuit schematics and implementation. (a) The islands of the device are labeled by the indices 1–3. Islands 1 and 2 are connected by a tunnel junction with Josephson energy E_{J} and capacitance C_{J}, shunted by a grAl inductance L_{q} and a capacitance C_{sh}, to form a generalized flux qubit. By connecting the third island to the qubit loop via the inductance L_{r}, we engineer the readout mode that charges the islands 1 and 2 in-phase. The qubit-readout coupling is controlled via the inductance asymmetry Δ_{k} between the loop branches. The capacitances C_{r} load the readout mode and C_{c} couples the circuit to the readout port. The colors indicate the materials used: blue for aluminum, red for grAl, and purple for aluminum covered with grAl as a result of the three-angle fabrication process. (b) Design layout of the device. The C_{c} pad has a skeletal shape to minimize screening currents and trapped vortices. (c) False-colored scanning electron micrograph of the qubit loop. By adjusting the length and width of the grAl strips, the resonator frequency, coupling strength, and qubit spectrum can be tuned independently. The insets show the Al/AlO$_x$/Al junction with an area of $A_{\text{J}} \approx 0.06\ \mu\text{m}^2$ and a section of the grAl wire. The grainy texture is due to a gold film deposited for imaging. (d) Schematics of the microwave reflection measurement setup at 10 mK.

implements a generalized flux qubit (GFQ).[33] The loop inductance L_{q} defines the inductive energy $E_{\text{L}} = \Phi_0^2/4\pi^2 L_{\text{q}}$ of the qubit, where $\Phi_0 = h/2e$ is the magnetic flux quantum.

If the circuit is symmetric with respect to the vertical symmetry line through node 3, which means that nodes 1 and 2 have equal capacitances C_{r} as well as equal inductances $L_{\text{q}}/2$, the qubit and resonator modes are electromagnetically uncoupled. The main stray capacitances of the design are discussed in the supplementary material.

The current in the readout mode splits between the qubit loop branches and in the case of perfect symmetry the net shared current with the qubit mode is zero. To engineer qubit-readout coupling, we introduce the kinetic inductive asymmetry $\Delta_{\text{k}} = \Delta_{\square} L_{\square}/2$ by designing different grAl inductor lengths for the two qubit inductors in the qubit loop with a total difference of $\Delta_{\square}$ squares of grAl wire with sheet inductance $L_{\square}$. In the case of JJ arrays, this would translate into using different junction numbers or junction sizes for the two inductors. As a result, the readout mode current splits unevenly in the qubit loop and the circuit is equivalent to an inductively coupled qubit,[34] where Δ_{k} plays the role of the shared inductance.

In contrast to capacitive[35,36] or conventional inductive[31,34] coupling of flux qubits, one circuit node is eliminated by collapsing the readout mode into the qubit loop. We would like to highlight several practical advantages of this coupling scheme. First, removing a circuit node pushes the parasitic modes to higher frequencies, improving the spectral purity of the device. Second, by coupling the resonator mode capacitively to a readout line using the capacitance C_c at node 3, the direct coupling of the qubit mode remains minimal thanks to the axial symmetry. Third, the qubit–resonator coupling can be designed to be purely inductive, loosening constraints on capacitor design, and possibly facilitating innovative flux-pumping schemes.[24]

We model Fig. 1(a) circuit in the harmonic oscillator basis of the linearized circuit eigenmodes,

$$\mathcal{H} = \hbar\omega_{\text{R}}\left(\hat{a}_{\text{R}}^{\dagger}\hat{a}_{\text{R}} + \frac{1}{2}\right) + \hbar\omega_{\text{Q}}\left(\hat{a}_{\text{Q}}^{\dagger}\hat{a}_{\text{Q}} + \frac{1}{2}\right) - E_{\text{J}}\cos\left(\lambda_{\text{R}}(\hat{a}_{\text{R}} + \hat{a}_{\text{R}}^{\dagger}) + \lambda_{\text{Q}}(\hat{a}_{\text{Q}} + \hat{a}_{\text{Q}}^{\dagger}) - \frac{2\pi}{\Phi_0}\Phi_{\text{ext}}\right), \quad (1)$$

where E_{J} is the Josephson energy, and $\hat{a}_{\text{R,Q}}^{\dagger}$ and $\hat{a}_{\text{R,Q}}$ are the bosonic creation and annihilation operators for the readout and qubit modes with eigenfrequencies ω_{R} and ω_{Q}, calculated without the Josephson inductance. The qubit and readout modes are linear combinations of the common and differential modes, defined by the dimensionless coupling coefficients $\lambda_{\text{R,Q}}$, derived in the supplementary material. If we neglect the nonlinearity of the granular aluminum wire, the JJ is the sole source of nonlinearity in the system, such that the intuitive picture of a nonlinear qubit and linear readout mode is justified for $\lambda_{\text{R}} \ll \lambda_{\text{Q}}$. Note that the coupling between readout and qubit vanishes for perfect symmetry, i.e., $\lambda_{\text{R}} \to 0$ for $\Delta_{\text{k}} \to 0$.

In Fig. 1(b), we show the layout of the qubit–resonator design. A scanning electron micrograph of the qubit loop is shown in Fig. 1(c). The qubit parameters can be tuned independently by adapting the length of the inductor L_{q}, the junction area defining E_{J} and C_{J}, and the size of the shunt capacitor electrodes determining C_{sh}. This can be done entirely geometrically, without changing the circuit topology nor the oxidation parameters for the JJ or the grAl film. The lateral inset in Fig. 1(c) shows a section of the grAl wire. Thanks to the relatively large kinetic inductance offered by grAl,[37,38] it is sufficient to add a few

squares of grAl film to one qubit branch to span the range from zero up to several nH of inductive asymmetry Δ_k. Notably, this can be done with minimal disturbance to the geometric inductance and the capacitance matrix.

The central inset of Fig. 1(c) shows a scanning electron micrograph of the qubit Al/AlO$_x$/Al junction. The entire device is fabricated on a c-plane sapphire substrate in a single lithographic step using a three-angle shadow evaporation technique, similar to Ref. 31. The aluminum layers (20 and 30 nm) are shadow evaporated to define the junction, followed by a zero-angle deposition of a 70 nm layer of grAl with resistivities between 450 and 1000 μΩcm depending on the device (cf. supplementary material). The sample is mounted in a modular flip-chip architecture, anchored to the baseplate of a dilution-cryostat at approximately 10 mK and it is measured in reflection, as shown in Fig. 1(d). The output signal is amplified using a dimer Josephson junction array amplifier (DJJAA)[39] operating close to the quantum noise limit.

We measure the spectra of 14 different GFQs as a function of the external flux Φ_{ext} using two-tone spectroscopy. A typical spectrum is shown in Fig. 2(a). Using the circuit Hamiltonian in Eq. (1) we fit the qubit and resonator spectra simultaneously to obtain the circuit parameters L_r, L_q, Δ_k, C_J, and E_J, while capacitors C_r and C_{sh} are inferred from finite-element simulations (see the supplementary material). The coupling asymmetry Δ_k is determined by the width of the avoided level crossing and L_q, C_J, and E_J are given by the measured qubit level structure.

The qubit spectra can be understood in terms of universal double-well physics,[33] ranging from the fluxon-tunneling regime $E_J > E_L$ in which the barrier height exceeds the confining quadratic potential, to the single-well plasmon regime for $E_J < E_L$. As summarized in Fig. 2(b), the distribution of qubit frequencies and anharmonicities follow the underlying single and double-well physics: Toward the plasmon regime, the qubit frequencies increase whereas the anharmonicities decrease. Toward the fluxon regime, frequencies decrease

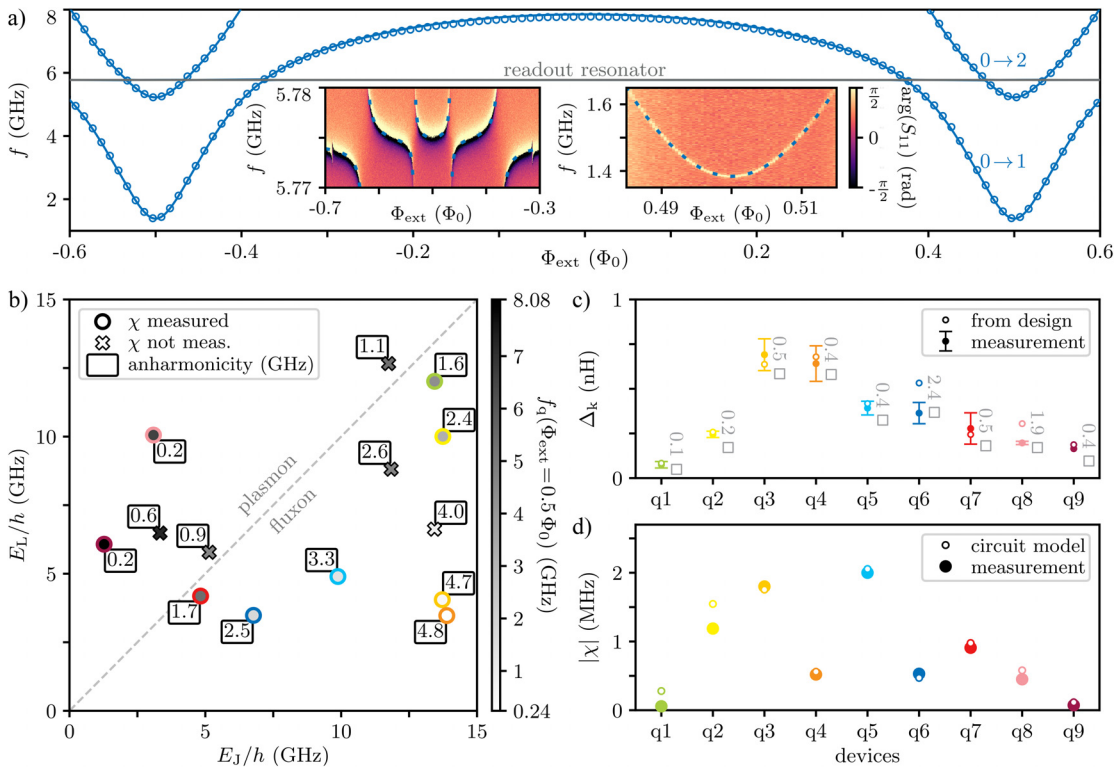

FIG. 2. From plasmon to fluxon: summary of measured qubit parameters. (a) Combined plot of typical single- and two-tone spectroscopy of 0 → 1 and 0 → 2 qubit transitions (blue circles) vs flux bias Φ_{ext} of device q6 as well as the 5.77 GHz resonance of the readout resonator (gray horizontal line). The inset on the left shows the measured phase response arg(S_{11}) of the readout mode in the vicinity of the qubit-readout avoided level crossings when probing the system with a single tone. The inset on the right shows the phase response of the resonator on resonance when probing the qubit with a second tone near the qubit frequency in the vicinity of the half-flux sweet spot $\Phi_{ext} = \Phi_0/2$. The blue lines (dashed and continuous) correspond to the fitted circuit model with fit parameters E_J, L_q, L_r, C_J, and Δ_k. (b) Phase diagram E_L vs E_J for the measured GFQs. The gray-scale intensity of the marker filler indicates the 0 → 1 transition frequency f_q at the half-flux point, with corresponding labels indicating the anharmonicity. The diagonal gray line separates the plasmon regime on the left from the fluxon regime on the right. Devices for which the dispersive shift χ was measured (was not measured) have a circular (cross-shaped) marker. (c) Qubit loop asymmetry Δ_k for selected devices. The filled circles indicate the values of Δ_k extracted from the joint fit of the qubit and resonator spectroscopy [cf. left inset of panel (a) and supplementary material]. The error bars correspond to possible capacitive coupling arising from asymmetries $\Delta_C = \pm 25$ aF $< 0.01 \times C_r$ in the capacitance matrix. The design values, shown as empty circles, are given by the product of the sheet inductance and the length difference between the qubit branches. The sheet inductance is extracted from the fitted L_q and the designed number of squares in the loop. The discrepancy between the measured and design values is shown in gray labels in units of squares. The marker color assigned to each sample is consistent in all panels. (d) Qubit state dependent dispersive shift χ at $\Phi_{ext} = \Phi_0/2$ for selected devices. Filled circles show χ values extracted from complex plane distributions of single shot measurements (cf. supplementary material). Empty circles indicate the calculated χ assuming pure kinetic inductance coupling.

while anharmonicities increase as expected from the exponential scaling of the qubit frequency with the barrier height.[40] At half-flux bias, we measure coherence times in the range of 1–10 μs, likely limited by inductive losses in grAl as summarized in the supplementary material.

In Fig. 2(c), we compare the fitted and designed coupling asymmetry Δ_k. The qubit-readout coupling is given by the sum of designed inductive coupling via Δ_k and spurious capacitive asymmetries, which we parametrize as $\Delta_C = (C_{13} - C_{23})/2$. These asymmetries can arise from asymmetric spurious capacitances of islands 1 and 2 to ground. From finite-element simulations, we estimate a maximal value of $\Delta_C = \pm 25$ aF due to a possible asymmetric displacement of the qubit chip with respect to ground. The corresponding uncertainties in the extraction of Δ_k are given as error bars in Fig. 2(c).

The dispersive shift of the readout resonator is

$$\chi = (E_{|1,1\rangle} - E_{|0,1\rangle})/h - (E_{|1,0\rangle} - E_{|0,0\rangle})/h,$$

where $E_{|n_R,n_Q\rangle}$ is the energy level sorted by the readout (n_R) and qubit (n_Q) photon number. In Fig. 2(d), we compare the measured dispersive shifts to the expected model values using the extracted Δ_k from spectroscopic measurements for nine qubits. The measured data are consistent with circuit model predictions for $\Delta_C = 0$, validating the pure kinetic inductance coupling design.

To quantify the readout performance of our device, we have performed two sets of characterization: contiguous measurement correlations and active state reset, with pulse sequences detailed in Figs. 3(a) and 3(e), respectively. We define the signal-to-noise ratio (SNR) in the I–Q plane of the readout mode as the distance between pointer states corresponding to qubit in $|0\rangle$ and $|1\rangle$ divided by the sum of their standard deviations. In all experiments, we fix SNR ≈ 3.7, which is obtained by adjusting the integration times $t_{int} \in (1600, 208)$ ns depending on the different average photon numbers $\bar{n} \in (10, 150)$ in the resonator.

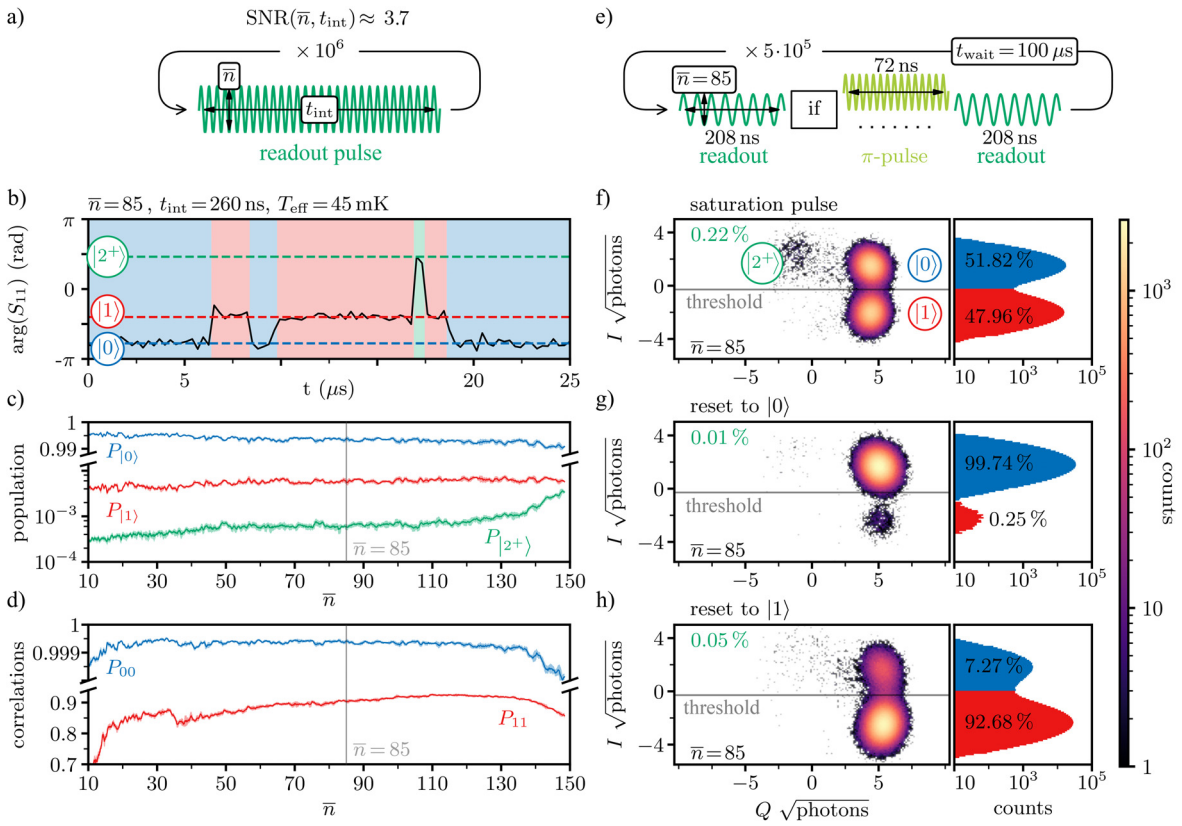

FIG. 3. Readout fidelity and quantum state preparation. (a) Pulse sequence for the continuous-wave measurement protocol: 10^6 contiguous readout pulses are sent and integrated for different photon numbers n. For each n, the integration time t_{int} is adapted to keep the SNR $= 3.7 \pm 0.2$. (b) Typical quantum jump trajectory visible in the measured phase of the reflection coefficient S_{11} shown in a window of 25 μs for device q7. The qubit states are assigned using a Gaussian mixture model and indicated by the color of the background: blue ($|0\rangle$ = ground), red ($|1\rangle$ = excited), and green ($|2^+\rangle$ = other). (c) Measured states population vs n. Note that leakage to the $|2^+\rangle$-states accelerates for $n \gtrsim 130$. (d) Correlation P_{xx} for consecutive measurements in the ground ($x = 0$) or excited ($x = 1$) state vs n. The minimal integration time, 200 ns, is approximately three times larger than the resonator response time. (e) Pulse sequence used for active state reset. The measurement outcome of the first readout pulse is used to condition a π-pulse on the qubit. The result of the second readout is used to assess the fidelity of the reset protocol. We use $n = 85$ and $t_{int} = 208$ ns resulting in a state separation of $\approx 6\sigma$. We repeat the sequence 5×10^5 times with a waiting time of $t_{wait} = 100$ μs in between. The measured pointer state distributions for 50% polarization, active reset to $|0\rangle$ and $|1\rangle$ are shown in panels (f)–(h), respectively. The gray line is the threshold used for state assignment in the active reset protocol. The green label indicates leakage into higher states. The measurement outcomes are depicted as histograms in logarithmic scale.

In Fig. 3(b), we show an example section of a contiguously measured quantum jump trace for GFQ device q7. By applying a Gaussian mixture model to quantum jump traces with 10^6 points for a given $\bar{n}$, we extract qubit populations in $|0\rangle$, $|1\rangle$, and $|2^+\rangle$ [see Fig. 3(c)] and correlations P_{00} and P_{11} for two successive measurements in the ground and excited state [see Fig. 3(d)], respectively. The correlations P_{00} and P_{11} serve as a measure of qubit-readout fidelity, particularly useful to assess quantum demolition effects introduced by the readout drive. Similarly to Ref. 41, the resilience of the grAl GFQ to readout-induced leakage[42–44] is illustrated by the fact that up to $\bar{n} \approx 100$, the qubit populations remain approximately constant, corresponding to an effective temperature of about 40–45 mK and residual excitations outside of the computational subspace remain below 0.1%.

Within the qubit subspace, we observe a significant difference in the correlation of successive readout outcomes when the qubit is in the ground or excited state. Qubit measurements in the ground state are highly correlated, with $P_{00} > 99.9\,\%$ for a broad range of readout powers. In contrast, we find that P_{11} depends on the readout strength, with $P_{11} \geq 90\,\%$ for $\bar{n} \in (75, 140)$. The difference between the measured P_{11} and perfect correlation can be accounted for by summing three contributions: Energy decay during the measurement reduces P_{11} by $1 - \exp(-t_{\mathrm{int}}/T_1)$, which for $t_{\mathrm{int}} = 352$ ns can be as high as 6% given the measured $T_1 = 8.0 \pm 2.4$ µs for device q7. Second, the qubit spectral shift and broadening induced by the readout tone will change the dissipative environment of the qubit[45] and might accelerate the relaxation from the excited to the ground state. The third contribution comes from demolishing effects activated when increasing $\bar{n}$,[46] such as leakage outside of the qubit subspace.[42] The second and third contributions, which sum up to give at least 4% of the P_{11} infidelity, provide a measure for the performance of the qubit-readout coupling scheme and motivate future research efforts.

We implement active state preparation starting from the thermal state of the qubit by playing a conditional π-pulse. The threshold to discriminate states $|0\rangle$ and $|1\rangle$ is determined by measuring the I–Q plane distributions after a saturation pulse, as shown in Fig. 3(f). Using $\bar{n} = 85$, the fidelities to reset the qubit to its ground and excited states read $P_0^{\mathrm{active}} = 99.7\%$ and $P_1^{\mathrm{active}} = 92.7\%$, respectively [cf. Figs. 3(g) and 2(h)]. In the error budget for quantum state preparation, the fidelity of the π-pulse of >99% (cf. supplementary material) is a negligible contribution compared to the decay during readout and quantum demolition effects. The measured performance for our GFQ devices are similar to the results reported for fluxoniums and transmons[41,47,48] but below state-of-the-art fidelity reaching 99%.[49] Currently, the main limitation for the readout performance is the energy relaxation time of the qubit, which can be significantly improved via material and design optimization.[50]

We have demonstrated dispersive coupling between a harmonic mode and a generalized flux qubit consisting of a single junction shunted by a granular aluminum inductor. By embedding the harmonic readout mode into the high kinetic inductance loop of the flux qubit, we implement a mechanism conceptually equivalent to inductive coupling, where the loop asymmetry is equivalent to the shared inductance. We validate the kinetic inductance coupling concept by comparing the spectra of 14 devices obtained via two-tone spectroscopy to a model including parasitic capacitances. We assess the suitability of the coupling mechanism for dispersive readout by performing quantum non-demolition readout with >90 % active state preparation fidelity and less than 0.1% leakage outside the qubit computational space. Thanks to its ability to provide a local qubit–resonator interaction unaffected by on-chip capacitors, we believe that the minimalist qubit–resonator design presented here will provide an advantageous avenue for up-scaling superconducting quantum devices.

See the supplementary material for a more detailed overview of the theoretical circuit models including corresponding finite-element simulations, the fabrication procedure, measured spectra, qubit coherence times, and time-domain pulse calibration techniques.

We are grateful to L. Radtke and S. Diewald for technical assistance. We acknowledge funding from the European Commission (FET-Open AVaQus GA 899561). Facilities use was supported by the KIT Nanostructure Service Laboratory. We acknowledge the use of measurement software framework qKit. The authors acknowledge support by the state of Baden-Württemberg through bwHPC. M.S., P.P, N.G., and T.R. acknowledge support from the German Ministry of Education and Research (BMBF) within the project GEQCOS (FKZ: 13N15683). D.B. and M.F. acknowledge funding from the German Federal Ministry of Education and Research (BMBF) within the project QSolid (FKZ: 13N16151). N.Z. acknowledges funding from the Deutsche Forschungsgemeinschaft (DFG—German Research Foundation) under Project No. 450396347 (GeHoldeQED). S.Gü., D.R., and W. W. acknowledge support from the Leibniz award WE 4458-5.

AUTHOR DECLARATIONS

Conflict of Interest

The authors have no conflicts to disclose.

Author Contributions

Simon Geisert and Soeren Ihssen contributed equally to this work.

Simon Geisert: Conceptualization (equal); Data curation (equal); Formal analysis (equal); Methodology (equal); Resources (equal); Software (equal); Validation (equal); Visualization (equal); Writing – original draft (equal); Writing – review & editing (equal). **Soeren Ihssen:** Conceptualization (equal); Data curation (equal); Formal analysis (equal); Methodology (equal); Resources (equal); Software (equal); Validation (equal); Visualization (equal); Writing – original draft (equal); Writing – review & editing (equal). **Patrick Winkel:** Conceptualization (equal); Methodology (equal); Resources (equal); Supervision (equal); Validation (equal); Writing – review & editing (equal). **Martin Spiecker:** Conceptualization (equal); Formal analysis (equal); Methodology (equal); Resources (equal); Validation (equal); Writing – review & editing (equal). **Mathieu Féchant:** Methodology (equal); Writing – review & editing (equal). **Patrick Paluch:** Methodology (equal); Resources (equal); Writing – review & editing (equal). **Nicolas Gosling:** Data curation (equal); Resources (equal); Software (equal); Writing – review & editing (equal). **Nicolas Zapata:** Data curation (equal); Resources (equal); Writing – review & editing (equal). **Simon Guenzler:** Methodology (equal); Resources (equal); Writing – review & editing (equal). **Dennis Rieger:** Methodology

(equal); Resources (equal); Writing – review & editing (equal). **Denis Bénâtre:** Data curation (equal). **Thomas Reisinger:** Resources (equal); Supervision (equal); Writing – review & editing (equal). **Wolfgang Wernsdorfer:** Resources (equal); Supervision (equal); Writing – review & editing (equal). **Ioan M. Pop:** Conceptualization (equal); Data curation (equal); Formal analysis (equal); Funding acquisition (equal); Investigation (equal); Methodology (equal); Project administration (equal); Resources (equal); Software (equal); Supervision (equal); Validation (equal); Visualization (equal); Writing – original draft (equal); Writing – review & editing (equal).

DATA AVAILABILITY

The data that support the findings of this study are available from the corresponding author upon reasonable request.

REFERENCES

[1]A. Wallraff, D. I. Schuster, A. Blais, L. Frunzio, R.-S. Huang, J. Majer, S. Kumar, S. M. Girvin, and R. J. Schoelkopf, "Strong coupling of a single photon to a superconducting qubit using circuit quantum electrodynamics," Nature **431**, 162 (2004).

[2]A. Blais, A. L. Grimsmo, S. M. Girvin, and A. Wallraff, "Circuit quantum electrodynamics," Rev. Mod. Phys. **93**, 025005 (2021).

[3]Y. Sung, L. Ding, J. Braumüller, A. Vepsäläinen, B. Kannan, M. Kjaergaard, A. Greene, G. O. Samach, C. McNally, D. Kim, A. Melville, B. M. Niedzielski, M. E. Schwartz, J. L. Yoder, T. P. Orlando, S. Gustavsson, and W. D. Oliver, "Realization of high-fidelity CZ and *ZZ*-free iSWAP gates with a tunable coupler," Phys. Rev. X **11**, 021058 (2021).

[4]C. R. Conner, A. Bienfait, H.-S. Chang, M.-H. Chou, É. Dumur, J. Grebel, G. A. Peairs, R. G. Povey, H. Yan, Y. P. Zhong, and A. N. Cleland, "Superconducting qubits in a flip-chip architecture," Appl. Phys. Lett. **118**, 232602 (2021).

[5]S. Kosen, H.-X. Li, M. Rommel, D. Shiri, C. Warren, L. Grönberg, J. Salonen, T. Abad, J. Biznárová, M. Caputo, L. Chen, K. Grigoras, G. Johansson, A. F. Kockum, C. Križan, D. P. Lozano, G. J. Norris, A. Osman, J. Fernández-Pendás, A. Ronzani, A. F. Roudsari, S. Simbierowicz, G. Tancredi, A. Wallraff, C. Eichler, J. Govenius, and J. Bylander, "Building blocks of a flip-chip integrated superconducting quantum processor," Quantum Sci. Technol. **7**, 035018 (2022).

[6]Y. Wu, W.-S. Bao, S. Cao, F. Chen, M.-C. Chen, X. Chen, T.-H. Chung, H. Deng, Y. Du, D. Fan, M. Gong, C. Guo, C. Guo, S. Guo, L. Han, L. Hong, H.-L. Huang, Y.-H. Huo, L. Li, N. Li, S. Li, Y. Li, F. Liang, C. Lin, J. Lin, H. Qian, D. Qiao, H. Rong, H. Su, L. Sun, L. Wang, S. Wang, D. Wu, Y. Xu, K. Yan, W. Yang, Y. Yang, Y. Ye, J. Yin, C. Ying, J. Yu, C. Zha, C. Zhang, H. Zhang, K. Zhang, Y. Zhang, H. Zhao, Y. Zhao, L. Zhou, Q. Zhu, C.-Y. Lu, C.-Z. Peng, X. Zhu, and J.-W. Pan, "Strong quantum computational advantage using a superconducting quantum processor," Phys. Rev. Lett. **127**, 180501 (2021).

[7]F. Arute, K. Arya, R. Babbush, D. Bacon, J. C. Bardin, R. Barends, R. Biswas, S. Boixo, F. G. S. L. Brandao, D. A. Buell, B. Burkett, Y. Chen, Z. Chen, B. Chiaro, R. Collins, W. Courtney, A. Dunsworth, E. Farhi, B. Foxen, A. Fowler, C. Gidney, M. Giustina, R. Graff, K. Guerin, S. Habegger, M. P. Harrigan, M. J. Hartmann, A. Ho, M. Hoffmann, T. Huang, T. S. Humble, S. V. Isakov, E. Jeffrey, Z. Jiang, D. Kafri, K. Kechedzhi, J. Kelly, P. V. Klimov, S. Knysh, A. Korotkov, F. Kostritsa, D. Landhuis, M. Lindmark, E. Lucero, D. Lyakh, S. Mandrà, J. R. McClean, M. McEwen, A. Megrant, X. Mi, K. Michielsen, M. Mohseni, J. Mutus, O. Naaman, M. Neeley, C. Neill, M. Y. Niu, E. Ostby, A. Petukhov, J. C. Platt, C. Quintana, E. G. Rieffel, P. Roushan, N. C. Rubin, D. Sank, K. J. Satzinger, V. Smelyanskiy, K. J. Sung, M. D. Trevithick, A. Vainsencher, B. Villalonga, T. White, Z. J. Yao, P. Yeh, A. Zalcman, H. Neven, and J. M. Martinis, "Quantum supremacy using a programmable superconducting processor," Nature **574**, 505 (2019).

[8]P. Campagne-Ibarcq, P. Six, L. Bretheau, A. Sarlette, M. Mirrahimi, P. Rouchon, and B. Huard, "Observing quantum state diffusion by heterodyne detection of fluorescence," Phys. Rev. X **6**, 011002 (2016).

[9]Z. K. Minev, S. O. Mundhada, S. Shankar, P. Reinhold, R. Gutiérrez-Jáuregui, R. J. Schoelkopf, M. Mirrahimi, H. J. Carmichael, and M. H. Devoret, "To catch and reverse a quantum jump mid-flight," Nature **570**, 200 (2019).

[10]S. Léger, J. Puertas-Martínez, K. Bharadwaj, R. Dassonneville, J. Delaforce, F. Foroughi, V. Milchakov, L. Planat, O. Buisson, C. Naud, W. Hasch-Guichard, S. Florens, I. Snyman, and N. Roch, "Observation of quantum many-body effects due to zero point fluctuations in superconducting circuits," Nat. Commun. **10**, 5259 (2019).

[11]J. Stevens, D. Szombati, M. Maffei, C. Elouard, R. Assouly, N. Cottet, R. Dassonneville, Q. Ficheux, S. Zeppetzauer, A. Bienfait, A. N. Jordan, A. Auffèves, and B. Huard, "Energetics of a single qubit gate," Phys. Rev. Lett. **129**, 110601 (2022).

[12]S. Chakram, K. He, A. V. Dixit, A. E. Oriani, R. K. Naik, N. Leung, H. Kwon, W.-L. Ma, L. Jiang, and D. I. Schuster, "Multimode photon blockade," Nat. Phys. **18**, 879 (2022).

[13]N. Mehta, R. Kuzmin, C. Ciuti, and V. E. Manucharyan, "Down-conversion of a single photon as a probe of many-body localization," Nature **613**, 650 (2023).

[14]N. Roch, M. E. Schwartz, F. Motzoi, C. Macklin, R. Vijay, A. W. Eddins, A. N. Korotkov, K. B. Whaley, M. Sarovar, and I. Siddiqi, "Observation of measurement-induced entanglement and quantum trajectories of remote superconducting qubits," Phys. Rev. Lett. **112**, 170501 (2014).

[15]R. Vijay, D. H. Slichter, and I. Siddiqi, "Observation of quantum jumps in a superconducting artificial atom," Phys. Rev. Lett. **106**, 110502 (2011).

[16]J. Heinsoo, C. K. Andersen, A. Remm, S. Krinner, T. Walter, Y. Salathé, S. Gasparinetti, J.-C. Besse, A. Potočnik, A. Wallraff, and C. Eichler, "Rapid high-fidelity multiplexed readout of superconducting qubits," Phys. Rev. Appl. **10**, 034040 (2018).

[17]F. Swiadek, R. Shillito, P. Magnard, A. Remm, C. Hellings, N. Lacroix, Q. Ficheux, D. C. Zanuz, G. J. Norris, A. Blais, S. Krinner, and A. Wallraff, "Enhancing dispersive readout of superconducting qubits through dynamic control of the dispersive shift: Experiment and theory," arXiv:2307.07765 (2023).

[18]I. Takmakov *et al.*, "Minimizing the discrimination time for quantum states of an artificial atom," Phys. Rev. Appl. **15**(6), 064029 (2021).

[19]M. Hofheinz, H. Wang, M. Ansmann, R. C. Bialczak, E. Lucero, M. Neeley, A. D. O'Connell, D. Sank, J. Wenner, J. M. Martinis, and A. N. Cleland, "Synthesizing arbitrary quantum states in a superconducting resonator," Nature **459**, 546 (2009).

[20]G. Kirchmair, B. Vlastakis, Z. Leghtas, S. E. Nigg, H. Paik, E. Ginossar, M. Mirrahimi, L. Frunzio, S. M. Girvin, and R. J. Schoelkopf, "Observation of quantum state collapse and revival due to the single-photon Kerr effect," Nature **495**, 205 (2013).

[21]K. Geerlings, Z. Leghtas, I. M. Pop, S. Shankar, L. Frunzio, R. J. Schoelkopf, M. Mirrahimi, and M. H. Devoret, "Demonstrating a driven reset protocol for a superconducting qubit," Phys. Rev. Lett. **110**, 120501 (2013).

[22]K. W. Murch, U. Vool, D. Zhou, S. J. Weber, S. M. Girvin, and I. Siddiqi, "Cavity-assisted quantum bath engineering," Phys. Rev. Lett. **109**, 183602 (2012).

[23]S. Shankar, M. Hatridge, Z. Leghtas, K. M. Sliwa, A. Narla, U. Vool, S. M. Girvin, L. Frunzio, M. Mirrahimi, and M. H. Devoret, "Autonomously stabilized entanglement between two superconducting quantum bits," Nature **504**, 419 (2013).

[24]Y. Lu, A. Maiti, J. W. O. Garmon, S. Ganjam, Y. Zhang, J. Claes, L. Frunzio, S. M. Girvin, and R. J. Schoelkopf, "High-fidelity parametric beamsplitting with a parity-protected converter," Nat. Commun. **14**(1), 5767 (2023).

[25]J. P. Gambino, S. A. Adderly, and J. U. Knickerbocker, "An overview of through-silicon-via technology and manufacturing challenges," Microelectron. Eng. **135**, 73 (2015).

[26]D. R. W. Yost, M. E. Schwartz, J. Mallek, D. Rosenberg, C. Stull, J. L. Yoder, G. Calusine, M. Cook, R. Das, A. L. Day, E. B. Golden, D. K. Kim, A. Melville, B. M. Niedzielski, W. Woods, A. J. Kerman, and W. D. Oliver, "Solid-state qubits integrated with superconducting through-silicon vias," npj Quantum Inf. **6**, 59 (2020).

[27]J. A. Alfaro-Barrantes, M. Mastrangeli, D. J. Thoen, S. Visser, J. Bueno, J. J. A. Baselmans, and P. M. Sarro, "Highly-conformal sputtered through-silicon vias with sharp superconducting transition," J. Microelectromech. Syst. **30**, 253 (2021).

[28]J. Yu, Y. Zheng, S. Zhou, Q. Wang, S. Wu, H. Wu, T. Li, and J. Cai, "Indium-based flip-chip interconnection for superconducting quantum computing application," in 23rd International Conference on Electronic Packaging Technology (ICEPT) (2022).
[29]K. N. Smith, G. S. Ravi, J. M. Baker, and F. T. Chong, "Scaling superconducting quantum computers with chiplet architectures," in 55th IEEE/ACM International Symposium on Microarchitecture (MICRO) (2022).
[30]M. Field, A. Q. Chen, B. Scharmann, E. A. Sete, F. Oruc, K. Vu, V. Kosenko, J. Y. Mutus, S. Poletto, and A. Bestwick, "Modular superconducting qubit architecture with a multi-chip tunable coupler," arXiv:2308.09240 (2024).
[31]L. Grünhaupt, M. Spiecker, D. Gusenkova, N. Maleeva, S. T. Skacel, I. Takmakov, F. Valenti, P. Winkel, H. Rotzinger, W. Wernsdorfer, A. V. Ustinov, and I. M. Pop, "Granular aluminium as a superconducting material for high-impedance quantum circuits," Nat. Mater. **18**, 816–819 (2019).
[32]D. Rieger, S. Günzler, M. Spiecker, P. Paluch, P. Winkel, L. Hahn, J. K. Hohmann, A. Bacher, W. Wernsdorfer, and I. M. Pop, "Granular aluminium nanojunction fluxonium qubit," Nat. Mater. **22**, 194 (2023).
[33]F. Yan, Y. Sung, P. Krantz, A. Kamal, D. K. Kim, J. L. Yoder, T. P. Orlando, S. Gustavsson, and W. D. Oliver, "Engineering framework for optimizing superconducting qubit designs," arXiv:2006.04130 (2020).
[34]W. C. Smith, A. Kou, U. Vool, I. M. Pop, L. Frunzio, R. J. Schoelkopf, and M. H. Devoret, "Quantization of inductively shunted superconducting circuits," Phys. Rev. B **94**, 144507 (2016).
[35]V. E. Manucharyan, J. Koch, L. I. Glazman, and M. H. Devoret, "Fluxonium: Single cooper-pair circuit free of charge offsets," Science **326**, 113 (2009).
[36]F. Bao, H. Deng, D. Ding, R. Gao, X. Gao, C. Huang, X. Jiang, H.-S. Ku, Z. Li, X. Ma, X. Ni, J. Qin, Z. Song, H. Sun, C. Tang, T. Wang, F. Wu, T. Xia, W. Yu, F. Zhang, G. Zhang, X. Zhang, J. Zhou, X. Zhu, Y. Shi, J. Chen, H.-H. Zhao, and C. Deng, "Fluxonium: An alternative qubit platform for high-fidelity operations," Phys. Rev. Lett. **129**, 010502 (2022).
[37]H. Rotzinger, S. T. Skacel, M. Pfirrmann, J. N. Voss, J. Münzberg, S. Probst, P. Bushev, M. P. Weides, A. V. Ustinov, and J. E. Mooij, "Aluminium-oxide wires for superconducting high kinetic inductance circuits," Supercond. Sci. Technol. **30**, 025002 (2016).
[38]L. Grünhaupt, N. Maleeva, S. T. Skacel, M. Calvo, F. Levy-Bertrand, A. V. Ustinov, H. Rotzinger, A. Monfardini, G. Catelani, and I. M. Pop, "Loss mechanisms and quasiparticle dynamics in superconducting microwave resonators made of thin-film granular aluminum," Phys. Rev. Lett. **121**, 117001 (2018).
[39]P. Winkel, I. Takmakov, D. Rieger, L. Planat, W. Hasch-Guichard, L. Grünhaupt, N. Maleeva, F. Foroughi, F. Henriques, K. Borisov, J. Ferrero, A. V. Ustinov, W. Wernsdorfer, N. Roch, and I. M. Pop, "Nondegenerate parametric amplifiers based on dispersion-engineered Josephson-junction arrays," Phys. Rev. Appl. **13**, 024015 (2020).
[40]G. Rastelli, I. M. Pop, and F. W. J. Hekking, "Quantum phase slips in Josephson junction rings," Phys. Rev. B **87**, 174513 (2013).
[41]D. Gusenkova, M. Spiecker, R. Gebauer, M. Willsch, D. Willsch, F. Valenti, N. Karcher, L. Grünhaupt, I. Takmakov, P. Winkel, D. Rieger, A. V. Ustinov, N. Roch, W. Wernsdorfer, K. Michielsen, O. Sander, and I. M. Pop, "Quantum nondemolition dispersive readout of a superconducting artificial atom using large photon numbers," Phys. Rev. Appl. **15**, 064030 (2021).
[42]M. F. Dumas, B. Groleau-Paré, A. McDonald, M. H. Muñoz-Arias, C. Lledó, B. D'Anjou, and A. Blais, "Unified picture of measurement-induced ionization in the transmon," arXiv:2402.06615 (2024).
[43]R. Shillito, A. Petrescu, J. Cohen, J. Beall, M. Hauru, M. Ganahl, A. G. Lewis, G. Vidal, and A. Blais, "Dynamics of transmon ionization," Phys. Rev. Appl. **18**, 034031 (2022).
[44]J. Cohen, A. Petrescu, R. Shillito, and A. Blais, "Reminiscence of classical chaos in driven transmons," PRX Quantum **4**, 020312 (2023).
[45]T. Thorbeck, Z. Xiao, A. Kamal, and L. C. G. Govia, "Readout-induced suppression and enhancement of superconducting qubit lifetimes," Phys. Rev. Lett. **132**, 090602 (2024).
[46]T. Walter, P. Kurpiers, S. Gasparinetti, P. Magnard, A. Potočnik, Y. Salathé, M. Pechal, M. Mondal, M. Oppliger, C. Eichler, and A. Wallraff, "Rapid high-fidelity single-shot dispersive readout of superconducting qubits," Phys. Rev. Appl. **7**, 054020 (2017).
[47]M. O. Tholén, R. Borgani, G. R. Di Carlo, A. Bengtsson, C. Križan, M. Kudra, G. Tancredi, J. Bylander, P. Delsing, S. Gasparinetti, and D. B. Haviland, "Measurement and control of a superconducting quantum processor with a fully integrated radio-frequency system on a chip," Rev. Sci. Instrum. **93**, 104711 (2022).
[48]D. Ristè, C. C. Bultink, K. W. Lehnert, and L. DiCarlo, "Feedback control of a solid-state qubit using high-fidelity projective measurement," Phys. Rev. Lett. **109**, 240502 (2012).
[49]Y. Sunada, S. Kono, J. Ilves, S. Tamate, T. Sugiyama, Y. Tabuchi, and Y. Nakamura, "Fast readout and reset of a superconducting qubit coupled to a resonator with an intrinsic purcell filter," Phys. Rev. Appl. **17**, 044016 (2022).
[50]I. Siddiqi, "Engineering high-coherence superconducting qubits," Nat. Rev. Mater. **6**, 875 (2021).